
# JOINT INSTITUTE FOR AERONAUTICS AND ACOUSTICS

National Aeronautics and
Space Administration

**Ames Research Center**

NASA-CR-166182
19810012486

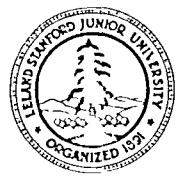

**Stanford University**



## JIAA TR - 32

# A SEMI-ANALYTIC APPROACH TO THE SELF-INDUCED MOTION OF VORTEX SHEETS

**Leonard W. Schwartz**

**MAY 1980**


The work here presented has been supported by the
National Aeronautics and Space Administration under Contract
NASA NCC 2-55

JIAA TR - 32

# A SEMI-ANALYTIC APPROACH TO THE SELF-INDUCED MOTION OF VORTEX SHEETS

LEONARD W. SCHWARTZ

MAY 1980

The work here presented has been supported by the National Aeronautics and Space Administration under Contract NASA NCC 2-55

TABLE OF CONTENTS

SUMMARY . . . . . iv

1. Introduction . . . . . 1

2. Mathematical Formulation . . . . . 7

3. Discussion of Results . . . . . 17

REFERENCES . . . . . 29

TABLE I . . . . . 31

TABLE II . . . . . 32

Figure 1 . . . . . 33

Figure 2 . . . . . 34

Figure 3 . . . . . 35

Figure 4 . . . . . 36

Figure 5 . . . . . 37

Figure 6 . . . . . 38

A SEMI-ANALYTIC APPROACH TO THE
SELF-INDUCED MOTION OF VORTEX SHEETS


## SUMMARY

The rolling-up of the trailing vortex sheet produced by a wing of finite span is calculated as a series expansion in time. For a vorticity distribution corresponding to a wing with cusped tips, the shape of the sheet is found by summing the series using Padé approximants. The sheet remains analytic for some time but ultimately develops an exponential spiral at the tips. The centroid of vorticity is conserved to high accuracy.

## 1. Introduction

Within the context of the potential theory of fluid motion surfaces of velocity discontinuity may be characterized as vortex sheets. Typically a shear layer in a real fluid is idealized by collapsing the region of large velocity gradient onto a sheet across which the magnitude and/or direction of the fluid velocity experiences a finite jump. The effects of viscosity are not considered; thus this concentrated vorticity cannot diffuse and the sheet will remain of zero thickness for all time. The sheet can, however, deform and stretch under the influence of its own induced velocity field. For example the vortex tube surrounding the circular jet has been observed to "roll up" into periodic spirals. Similar behavior has also been observed in the two-dimensional analogue. Rosenhead (1931) introduced a discrete vortex approximation to study the time evolution of a sinusoidally perturbed two-dimensional vortex sheet across which the velocity jumps discontinuously. The continuous sheet is replaced by a line of point vortices whose strengths vary sinusoidally. The induced velocity at a given point vortex, at any instant in time, is given by the vector sum of the contributions from all the others. In the initial stages of motion, at least, the rolling-up phenomenon is clearly indicated in his results. Not all vortex sheets must deform, however. Two-dimensional gravity waves may propagate without change of form on the interface between two fluids of different constant density. Within each fluid the motion is irrotational with a discontinuity in speed across the interface. The search for a wave of con-

stant form may be thought of as the determination of that particular vortex sheet configuration which preserves its "initial" shape.

A particular vortex sheet whose evolution has been a topic of extensive study is that left in the wake of a lifting surface or wing. The span-wise distribution of vorticity in the sheet is produced by the shedding of vortex lines as the lift varies along the wing from centerline to tip. A classical two-dimensional problem is obtained by considering the self-induced motion in a plane so far behind the wing that the bound vorticity produces negligible effect (the "Trefftz-plane"). Thus Westwater (1936) computed the two-dimensional motion of a sheet of finite span, that is initially flat, with the variation of vorticity produced by a wing on which the lift varies elliptically. Following Rosenhead, he used the discrete vortex approximation using 10 point vortices of the same strength distributed along a semi-span. Each vortex is placed initially at the centroid of vorticity of the segment of the distribution it replaces. His results suggest an orderly rolling-up pattern starting at the edges. Earlier, Kaden (1931) found an analytic expression for the form of the sheet in the neighborhood of the edge. He considered a semi-infinite sheet of vorticity produced by the parabolic lift variation that approximates the elliptic variation at the edge. Because there is no characterisitc length in the field, Kaden was able to extract a simple similarity solution for the shape that, in polar coordinates, is a spiral whose form is given approximately by

$$r = \left[\frac{\kappa t}{\pi\theta}\right]^{2/3}$$

where $t$ is time. This is a tightly-wound spiral of infinite length, a typical dimension of which grows as $t^{2/3}$. Kaden's results confirm a still earlier prediction of Prandtl (1927) that vortex sheets behind wings will roll up towards their tips. Because Kaden's similarity solution suggests that the spiral is always completely wound up, even at $t = 0^+$, the sheet, while sensibly flat at $t = 0$, is, in fact, higher singular at the tip.

With the advent of automatic computing, it became possible to pursue the discrete-vortex or "multi-vortex" approximation in much greater detail. Takami (1964) and others were unable to reproduce Westwater's smooth roll-up results. Chaotic motion was observed near the tips even at the early stages of motion. Presumably the smooth patterns obtained by Westwater were due to fortuitous inaccuracy in his time-integration scheme. Even more disconcerting was the effect of increasing the number of discrete vortices. Rather than improve the results, the choatic motion was amplified. When two discrete vortices moved "too close" they induced inacceptibly large velocities upon each other. Takami also considered other distributions of vorticity including the one produced by a wing with cusped tips (3/2-power loading). In this case, the strength of the sheet goes to zero at the tips and smoother behavior might be expected. On the contrary, his results for this case indicate that the region of disorderly motion is not confined to the vicinity of the tips but extends over much of the sheet.

A serious criticism of the multi-vortex approximation was made by Birkhoff & Fisher (1959). They assert that the self-induced motion of an array of point vortices will ultimately produce randomness

of position and hence that no true rolling-up is possible. Perhaps motivated by this objection, several authors have modified the numerical problem through the introduction of various smoothing techniques. Thus Chorin & Bernard (1973), for example, introduce an arbitrary maximum on the permissible induced velocity and claim that this procedure reproduces some of the features of viscosity.

A significant step foward was made by Fink and Soh (1974, 1978). After carefully comparing the multi-vortex model with the original Cauchy principal-value integral, they concluded that the former involves the neglect of initially-small logarithmic terms. This error becomes amplified as the sheet moves and ultimately leads to the observed chaotic motions. Their improvement is simply to rediscretize at each time step. In a number of applications, including the rolling-up of a trailing vortex sheet, their results remain smooth for much longer periods of time than had been previously reported.

In addition to its inherent mathematical interest, the problem of trailing vortex-sheet roll-up is of significant practical importance. Spreiter & Sacks (1951) show that for heavily-loaded low-aspect-ratio wings, the sheet may become essentially rolled up into two vortex cores within a chord length of the wing trailing edge. This effect must be considered in a valid analysis of plane tail performance in these cases. Additional interest followed the introduction of wide-bodied transport planes with heavily loaded wings of high aspect ratio in the early 1970's. Strong vortex cores left by the passage of these large aircraft in the vicinity of airports have been implicated as a contributing factor to accidents involving smaller aircraft.

In the present work we seek to solve for the self-induced motion of a finite two-dimensional vortex sheet without introducing any discretization at all. The position of the vortex sheet is calculated as a power series in time with coefficients that are analytic functions of a curve parameter. Thus the procedure is restricted to those lift distributions that produce sheets whose motion is analytic in time initially.

In §2 we show that for a particular class of vorticity distributions $\kappa(x_o)$, the coefficients in the series will be polynomial functions of $x_o$ the curve parameter. For this class an algorithm to find the coefficients, suitable for machine computation, is worked out in detail. We pay particular attention to the case of 3/2-power lift distribution, i.e. $(1 - x_o^2)^{3/2}$ in dimensionless units. The corresponding vorticity $\kappa(x_o) = 3x_o\sqrt{1 - x_o^2}$ is the most singular distribution in the class for which the Hölder condition [see e.g. Muskhelishvili (1958)]

$$|\kappa(x_o)| < A|x_o - 1|^{\alpha}, \quad 0 < A < \infty, \quad 0 < \alpha < 1$$

is satisfied at the edge(s) of the sheet. The Hölder condition, which is stronger than continuty but weaker than differentiability, is sufficient to ensure existence of the Cauchy principal-value integrals from which the series coefficients are calculated.

Results of the algorithm developed in §2 are presented in §3. The series for the sheet coordinates is computed to $O(t^{42})$ for the 3/2-power lift case. The series have a finite radius of convergence; convergence fails first at the tips for a dimensionless value of time

of about 0.39. Using Padé approximants highly accurate sheet profiles are computed and are compared with the numerical work of Takami and Fink & Soh. The limiting singularity is associated with the instantaneous appearance of a loosely-wound spiral of finite length. Unlike Kaden's power-low spiral, the local solution here is

$$r = Ke^{-k\theta} \quad .$$

Once the spiral appears at the tip the analytic solution can no longer be used. One may conjecture, however, that, as time proceeds, vorticity is drawn into the vortex core until, ultimately, it is all concentrated there.

A useful check on the series solution is provided by the invariance of the horizontal coordinate of the vorticity centroid. Two separate checks can be formulated: one relating to a weighted sum of the series coefficients at any order and, secondly, a global check involving numerical integration of the Padé-summed series results. Both suggest that the present results are effectively exact until the critical time is reached.

Finally we compute the series solution that is associated with a slightly-perturbed elliptic lift variation. This "solution" is completely analytic and does not include the singularity at the tip at $t = 0$ . Thus it is incomplete, does not conserve the position of the centroid, but it may be useful as an "outer" solution for purposes of matching.

## 2. Mathematical Formulation

The velocity field induced at time t, by a vortex sheet with concentrated vorticity distribution $\tilde{\kappa}(s,t)$ where s is arc length, is given by

$$\bar{q}(z,t) = u - iv = -\frac{i}{2\pi}\int_c \frac{\tilde{\kappa}(s,t)ds}{z - z(s,t)} \qquad (1)$$

in the usual complex notation. The induced velocity at points on the sheet is also given by this expression if the Cauchy principal value of the integral is taken. $\tilde{\kappa}$ is, in fact, equal to the difference in the tangential components of velocity across the sheet. Assuming that, at the initial instant of time, the sheet lies on the x-axis between -b and b we introduce the line parameter $x_o \in [-b,b]$ and the "Lagrangian" vorticity distribution $\kappa(x_o)$ defined by

$$\tilde{\kappa}(s,t) = \kappa(x_o)\frac{dx_o}{ds}$$

Since the fluid is assumed to be inviscid, the time-dependence is only found in the sheet-stretching factor $dx_o/ds$. Equation (1) becomes, for points on the sheet,

$$u(x_o,t) - iv(x_o,t) = -\frac{1}{2\pi}\oint_{-b}^{b} \frac{\kappa(\xi)d\xi}{z(x_o,t) - z(\xi,t)} \quad . \qquad (2)$$

The lift distribution is taken to be bilaterally symmetric; hence $\kappa(x_o)$ is antisymmetric and we introduce the circulation about half the vortex sheet

$$\Gamma = \int_o^b \kappa(x_o)dx_o \quad . \qquad (3)$$

The problem may be made dimensionless be selecting $b$ as reference length and $b^2/\Gamma$ as reference time. Separately equating real and imaginary parts of (2) and recognizing that $u(x_o,t) = \frac{\partial}{\partial t} x(x_o,t)$ and $v(x_o,t) = \frac{\partial}{\partial t} y(x_o,t)$, we obtain the coupled system of nonlinear integro-differential equations

$$\frac{\partial}{\partial t} x(x_o,t) = -\frac{1}{2\pi} \oint_{-1}^{1} \frac{\kappa(\xi)\,[y(x_o,t) - y(\xi,t)]}{R^2}\, d\xi \tag{4a}$$

and

$$\frac{\partial}{\partial t} y(x_o,t) = \frac{1}{2\pi} \oint_{-1}^{1} \frac{\kappa(\xi)\,[x(x_o,t) - x(\xi,t)]}{R^2}\, d\xi \tag{4b}$$

where

$$R^2 = [x(x_o,t) - x(\xi,t)]^2 + [y(x_o,t) - y(\xi,t)]^2 \,. \tag{4c}$$

We shall now seek solutions of (4) which may be developed as power series in time that are uniformly convergent for $x_o \in [-1,1]$. Clearly if such solutions exist they must be of the form

$$x(x_o,t) = x_o + \sum_{i=1}^{\infty} A_i(x_o)\, t^{2i} \,, \tag{5a}$$

$$y(x_o,t) = \sum_{i=0}^{\infty} B_i(x_o)\, t^{2i+1} \,. \tag{5b}$$

If we further assume that the vorticity is of the form

$$K(\xi) = \frac{\xi}{\sqrt{1 - \xi^2}} \sum_{j=0}^{N} c_j \xi^{2j} \tag{6}$$

it can be shown that the coefficients $A_l$ and $B_l$ will be polynomial functions of their arguments. The dimensionless form of equation (3) requires that

$$c_o + \sum_{j=1}^{N} c_j \left( \frac{2 \cdot 4 \cdot 6 \cdots 2j}{3 \cdot 5 \cdot 7 \cdots (2j + 1)} \right) = 1 \quad .$$

The form (6) includes the elliptic lift distribution and the 3/2-power distribution produced by a cusped wing planform as special cases. It does not include the distributions characteristic of rectangular or lenticular planforms; indeed, no series development in time, starting from an initially flat sheet, is possible for these later cases.

When (5) and (6) are substituted in (4) and the coefficients of the various series in $t$ are collected, the Cauchy integrations can be performed using the family of "airfoil integrals"

$$\mathcal{I}_n = \int_{-1}^{1} \frac{\xi^n \, d\xi}{\sqrt{1 - \xi^2} \, (x_o - \xi)} \quad , \quad n = 1, 2, \ldots \tag{7}$$

The expressions for $\mathcal{I}_n(x_o)$ may be found recursively according to the scheme

$$\mathcal{I}_1 = -\pi$$

$$\mathcal{I}_n = x_o \ \mathcal{I}_{n-1} \quad (n \text{ even}) \tag{8}$$

$$\mathcal{I}_n = x_o \ \mathcal{I}_{n-1} - \pi \frac{1 \cdot 3 \cdot 5 \cdots (n-2)}{2 \cdot 4 \cdot 6 \cdots (n-1)} \quad (n \text{ odd}).$$

It is important to note that $\mathcal{I}_n(x_o)$ are defined only on the open interval (-1, 1).

The series expansion procedure will now be described in detail. Several intermediate variables will be introduced both for computational convenience and also to reduce the problem to one that is only quadratically nonlinear. We define $A_o \equiv x_o$ and let

$$C_i = A_i(x_o) - A_1(\xi), \tag{9}$$

and

$$D_i = B_i(x_o) - B_1(\xi). \tag{10}$$

From equation (4c),

$$R^2 = \sum_{k=0}^{\infty} E_k t^{2k} \tag{11}$$

where

$$E_k = \sum_{i=0}^{k} C_i C_{k-i} + \sum_{i=1}^{k} D_{i-1} D_{k-i} \ . \tag{12}$$

Let

$$\frac{y(x_o,t - y(\xi,t)}{R^2} = \sum_{j=0}^{\infty} F_j t^{2j+1} \tag{13}$$

and

$$\frac{x(x_o,t) - x(\xi,t)}{R^2} = \sum_{j=0}^{\infty} G_j t^{2j} \quad . \tag{14}$$

After equating coefficients of like powers of $t$, we obtain, from (13) and (14) respectively,

$$E_o F_l = D_l - \sum_{k=1}^{l} E_k F_{l-k} \quad , \tag{15}$$

$$E_o G_l = C_l - \sum_{k=1}^{l} E_k G_{l-k} \tag{16}$$

for all positive integers $l$. The summations are identically zero when $l = 0$. Finally we differentiate equations (5) with respect to $t$ and substitute into (4a) and (4b) to obtain

$$-4\pi(l + 1)\, A_{l+1} = \oint_{-1}^{1} \kappa(\xi) F_i \, d\xi \quad , \tag{17a}$$

$$2\pi(2l + 1)\, B_l = \oint_{-1}^{1} \kappa(\xi) G_l \, d\xi \quad , \tag{17b}$$

for $l \geq 0$.

Equations 9, 10, 12, and 15-17 form a complete system for the successive determination of the coefficients A,...,G. If $\kappa(\xi)$ is of the form (6), $A_i$ and $B_l$ will be polynomials in $x_o$ and $C_l$, $D_l$, $E_l$, $(x_o - \xi)F_l$ and $(x_o - \xi)G_l$ are polynomials in $x_o$ and $\xi$. The degree

of these polynomials, for each i, will increase, in general, with increasing N. If, for example, N = 1 in equation (6) it can be established by induction that a sufficient form is given by

$$A_i(x_o) = \sum_{j=0}^{i} \alpha_{ij} x_o^{2j+1} \quad , \tag{18a}$$

$$B_i(x_o) = \sum_{j=0}^{i+1} \beta_{ij} x_o^{2j} \quad , \tag{18b}$$

$$E_k = (x_o - \xi)^2 \sum_{t=0}^{2k} E_{kt}(x_o)\xi^t \quad , \tag{18c}$$

$$F_i = \frac{1}{(x_o - \xi)} \sum_{s=0}^{2i+1} F_{is}(x_o)\xi^s \quad , \tag{18d}$$

and

$$G_i = \frac{1}{(x_o - \xi)} \sum_{s=0}^{2i} G_{is}(x_o)\xi^s \quad , \tag{18e}$$

where

$$E_{kt} = \sum_{p=\left[\frac{t+1}{2}\right]}^{k} E_{ktp} x_o^{2p-t} \quad , \tag{18f}$$

$$F_{is} = \sum_{j=1+[s/2]}^{i+1} F_{isj} x_o^{2j-1-s} \quad , \tag{18g}$$

and

$$G_{is} = \sum_{j=\left[\frac{s+1}{2}\right]}^{i} G_{isj}\, x_o^{2j-s} \quad . \tag{18h}$$

Here $[\ ]$ denotes the integer-part function. Substituting (18a), (18b) and (18f) into (12) and using identities of the form

$$x_o^{2j} - \xi^{2j} = (x_o - \xi) \sum_{r=0}^{2j-1} x_o^{2j-1-r}\, \xi^r$$

to eliminate the explicit dependence on the intermediate variables $C_i$ and $D_i$ we obtain, after some manipulation,

$$E_{ktp} = \sum_{i=0}^{k} \sum_{j=\mathrm{Max}[0,p+i-k]}^{\mathrm{Min}[p,i]} \alpha_{ij}\, \alpha_{k-i,p-j}\, \gamma_{tpj} + \sum_{i=1}^{k} \sum_{j=\mathrm{Max}[1,p+i-k-1]}^{\mathrm{Min}[p,i]} \beta_{i-1,j}\, \beta_{k-i,p-j+1}\, \bar{\gamma}_{tpj} \quad . \tag{19}$$

The new functions introduced in (19) are defined by

$$\gamma_{tpj} = 1 + \mathrm{Min}[t, 2p-t, 2j, 2p-2j]$$

and $$\bar{\gamma}_{tpj} = \mathrm{Min}[t+1, 2p-t+1, 2j, 2p-2j+2].$$

Summations in (19) are taken to be identically zero when the lower limit exceeds the upper.

Expressions for the triply-subscripted elements $F_{isj}$ and $G_{isj}$ may be obtained from (15) and (16) as

$$\sum_{j=1+\left[s/2\right]}^{i+1} \left( F_{isj} - \beta_{ij} \right) x_o^{2j-1-s}$$

$$= -\sum_{k=1}^{i} \sum_{t=Max[0,s+2k-2i-1]}^{Min[2k,s]} \sum_{p=\left[\frac{t+1}{2}\right]}^{k} \sum_{m=1+\left[\frac{s-t}{2}\right]}^{i-k+1} E_{ktp} F_{i-k,s-t,m} x_o^{2p+2m-1-s}$$

$$(s = 0, 1, \ldots 2i + 1) \qquad (20)$$

and

$$\sum_{j=\left[\frac{s+1}{2}\right]}^{i} \left( G_{isj} - \alpha_{ij} \right) x_o^{2j-s}$$

$$= -\sum_{k=1}^{i} \sum_{t=Max[0,s+2k-2i]}^{Min[2k,s]} \sum_{p=\left[\frac{t+1}{2}\right]}^{k} \sum_{m=\left[\frac{s-t+1}{2}\right]}^{i-k} E_{ktp} G_{i-k,s-t,m} x_o^{2p+2m-s}$$

$$(s = 0, 1, \ldots 2i). \qquad (21)$$

Note that the last subscript in $F_{isj}$ and $G_{isj}$ on the left-hand side of (20) and (21) is given implicitly or computed from the exponents of $x_o$ in the quadruple sums. While explicit expressions similar to those obtained for $E_{ktp}$ in (19) are possible in principle, the present procedure is at least as efficient computationally and avoids a great deal of laborious analysis.

The system of equations for the coefficients is complete once the reduced form of equations (17) is obtained. For the special case of 3/2-power wing loading, $c_o = -c_1 = 3$, the induced velocities are continuous at the edges of the sheet and equations (17) can be written

in a relatively simple form. The relevant family of Cauchy integrals is

$$I_n = \frac{1}{\pi} \oint_{-1}^{1} \frac{\xi^n \sqrt{1-\xi^2}}{x_o - \xi} \, d\xi \quad , \quad n = 1, 2, \ldots$$

which are related to the original family according to

$$I_n = \frac{1}{\pi} \left( \mathcal{I}_n - \mathcal{I}_{n+2} \right) .$$

$I_n$ can be computed recursively as

$$I_1 = x_o^2 - 1/2 \quad ,$$

$$I_n = x_o I_{n-1} \qquad \text{(n even)} \quad ,$$

$$I_n = x_o I_{n-1} - \frac{1 \cdot 3 \cdot 5 \cdots (n-2)}{2 \cdot 4 \cdot 6 \cdots (n+1)} \qquad \text{(n odd)} \quad ,$$

from equation (8).

They are even or odd polynomials in $x_o$, of the form

$$I_n = \sum_{p=0}^{\left[\frac{n+1}{2}\right]} K_p \, x_o^{n+1-2p} \tag{22}$$

where $K_p$ are determined by

$$K_o = 1$$

$$K_{p+1} = \frac{2p-1}{2p+2} K_p \qquad p = 0, 1. \ldots \quad .$$

Equations (17) now become

$$\sum_{\ell=0}^{i+1} \alpha_{i+1,\ell}\, x_o^{2\ell+1} = -\frac{3}{4(i+1)} \sum_{s=0}^{2i+1} \sum_{j=1+\left[s/2\right]}^{i+1} \sum_{p=0}^{1+\left[s/2\right]} K_p F_{isj}\, x_o^{2(j-p)+1} \qquad (23)$$

and

$$\sum_{\ell=0}^{i+1} \beta_{i\ell} x_o^{2\ell} = \frac{3}{2(2i+1)} \sum_{s=0}^{2i} \sum_{j=\left[\frac{s+1}{2}\right]}^{i} \sum_{p=0}^{1+\left[s/2\right]} K_p G_{isj}\, x_o^{2(j-p)+2} \,. \qquad (24)$$

Starting with $\alpha_{10} = 1$ and $i = 0$, the five coefficient equations are solved in the order (19), (21), (24), (20), (23). The index $i$ is then incremented by one and the next order of calculation is performed.

## 3. Discussion of Results

The special case corresponding to the 3/2-power lift distribution has been computed to $O(t^{42})$ using an optimized FØRTRAN compiler on the Stanford IBM 370. Execution time for a solution of order $t^{2N}$ was found to be proportional to $N^5$ which is consistent with the number of nested summations in the algorithm of the last section. For $2N = 42$, the computation required 2.2 sec of CPU time. Double-precision (16-place) arithmetic was used and all coefficients are accurate to at least 4 places even at the highest order. Extended precision would be necessary however for a solution of still higher order.

Though $O(t^7)$ the coefficients in the double series for $x$ and $y$ can be recognized as rational numbers:

$$x(x_o,t) = x_o + x_o\left(\frac{9}{8} - \frac{9}{4}x_o^2\right)t^2 - x_o\left(\frac{135}{128} - \frac{135}{32}x_o^2 + \frac{27}{8}x_o^4\right)t^4 + x_o\left(\frac{8343}{5120} - \frac{31509}{2560}x_o^2 + \frac{4131}{160}x_o^4 - \frac{81}{5}x_o^6\right)t^6 + O(t^8)\,, \tag{25a}$$

$$y(x_o,t) = -\left(\frac{3}{4} - \frac{3}{2}x_o^2\right)t + \left(\frac{9}{32} - \frac{9}{8}x_o^4\right)t^3 - \left(\frac{81}{256} - \frac{81}{128}x_o^2 - \frac{81}{32}x_o^4 + \frac{567}{160}x_o^6\right)t^5 + \left(\frac{7047}{14336} - \frac{243}{112}x_o^2 - \frac{73629}{17920}x_o^4 + \frac{7533}{320}x_o^6 - \frac{90639}{4480}x_o^8\right)t^7 + O(t^9)\,. \tag{25b}$$

The coefficients in (25) through $0(t^4)$ agree with those calculated by Professor M. D. Van Dyke as reported by Takami (1964).

For a given value of $t$, the coordinates of a point $(x,y)$ lying on the vortex sheet can be found by summing the series in equations (5a) and (5b). Since only a finite number of terms in these series are known, their sum, for each value of $x_o$, can be approximated by considering the convergence of the sequence of "diagonal Padé approximants" formed from such series. Padé approximants are ratios of polynomials with coefficients so chosen so that, when expanded for small argument, the power series expansions of these ratios agree with the original series to appropriate order. Diagonal approximants have the additional property that the order of the numerator and denominator are equal. Thus if the power series for a function $f(\varepsilon)$ is known through $0(\varepsilon^{2N})$,

$$f(\varepsilon) = a_o + a_1\varepsilon + \ldots + a_{2N}\varepsilon^{2N} + 0(\varepsilon^{2N+1})$$

we can, in general, form an approximant, denoted by $[N/N]f$, so that

$$f(\varepsilon) = [N/N]f + 0(\varepsilon^{2N+1}),$$

where

$$[N/N]f = \frac{b_o + b_1\varepsilon + \ldots + b_N\varepsilon^N}{1 + c_1\varepsilon + \ldots + c_N\varepsilon^N},$$

and the $b_j$ and $c_j$ are determined uniquely from $a_o, \ldots, a_{2N}$ for given $N$. The sequence of approximants so formed will usually converge much faster than the original series and can converge to the analytic continuation of the series if $\varepsilon$ lies outside the radius

of convergence. A number of examples of the use of this technique in the solution of fluid mechanics problems can be found in Cabannes (1976).

Figure 1 shows two configurations of the vortex sheet drawn for $t^2 = .05$ and .15. These have been computed as [10/10] approximants to the $t^2$-series for $x(x_o,t)$ and $y(x_o,t)/t$. Also shown in the figure is the induced velocity profile at $t=0$ in arbitrary units. For $t^2 = .05$, the sequence of diagonal approximants converged to 14-decimal places for all $x_o$ in [0,1]. Even the [3/3] approximants constructed from only seven terms in each series in (5) agree to 7-decimal places with the converged results. For $t^2 = .15$, on the other hand, 5-place convergence was obtained for $x_o \leq 0.998$. We will show below that a singularity has appeared in the $t^2$-series to destroy convergence for $x_o$ slightly greater than this value. Notice that the sheet has curved back for $t^2 = .15$; the value of the parameter $x_o$ where the tangent to the sheet is vertical is about 0.975.

In Figure 2 we compare the results of the present method with the multi-vortex results of Takami (1964) and the numerical results of Fink and Soh (1974). Both authors have produced solutions for $t^2 = .16$. Takami's results exhibit the partial disorder characteristic of the simple multi-vortex representation. Fink and Soh have computed a smooth shape for the sheet that is in general agreement with the [10/10] approximant solution except near the tip of the sheet. Their relatively coarse point spacing is, apparently, unable to resolve the details in this region. In fact, the sheet exhibits

a singularity at $x_o \approx 0.997$ for this value of $t^2$. Convergence of the diagonal approximants failed for $x_o > .990$ and we have only drawn the sheet up to this point.

For a bilaterally symmetric vortex sheet it can be shown that the horizontal position of the centroid of vorticity, which in our parametric notation is defined by

$$X = \int_0^1 x(x_o,t)\kappa(x_o)dx_o \tag{26}$$

is an invariant of the motion. We have

$$\frac{dX}{dt} = \int_0^1 \frac{\partial x}{\partial t}(x_o,t)\kappa(x_o)dx_o \quad . \tag{27}$$

Using equation (4a), the right side of (27) can be written as

$$-\frac{1}{2\pi}\int_0^1 \kappa(x_o)dx_o \oint_{-1}^{1} \kappa(\xi)\,\frac{[y(x_o,t) - y(\xi,t)]}{R^2}\,d\xi$$

$$= -\frac{1}{2\pi}\left\{\int_0^1\oint_0^1 \kappa(x_o)\kappa(\xi)\frac{[y(x_o,t) - y(\xi,t)]}{R^2}\,d\xi\,dx_o \right. \tag{28}$$

$$\left. -\int_0^1\int_0^1 \frac{\kappa(x_o)\kappa(\xi)[y(x_o,t) - y(\xi,t)]\,d\xi\,dx_o}{[x(x_o,t) + x(\xi,t)]^2 + [y(x_o,t) - y(\xi,t)]^2}\right\}$$

where we have used the symmetry requirements $\kappa(-\xi) = -\kappa(\xi)$, $y(-\xi,t) = y(\xi,t)$, $x(-\xi,t) = -x(\xi,t)$ to obtain the last integral. Each integral on the right of (28) is invariant under the interchange of the dummy arguments $x_o$ and $\xi$ and hence is equal to zero.

The fact that $dX/dt$ is zero can be used in two different ways to check our solution. Substituting expansion (5a) in (27) we obtain immediately

$$\int_0^1 A_i(x_o)\kappa(x_o)\, dx_o = 0 , \quad i = 1, 2, \ldots .$$

With $A_i = \sum_{j=0}^{i} \alpha_{ij} x_o^{2j+1}$ and $\kappa = 3x_o\sqrt{1-x_o^2}$ , the integrations can be performed to yield a check on the sums of the coefficients at each order in $i$:

$$\sum_{j=0}^{i} \alpha_{ij} k_j = 0, \quad i = 1, 2, \ldots$$

where

$$k_j = \frac{1\cdot3\cdot5\cdots(2j+1)}{2\cdot4\cdot6\cdots(2j+4)} .$$

Performing this check numerically on $\alpha_{ij}$ produces a result for each $i$ that is at least 16 orders of magnitude less than the largest coefficients in the sum. Thus the solution satisfies the consistency relation at each order; we also have an estimate for the round-off error in the coefficients.

The invariance of $X$ can also be used to check the Padé-summed results for $x(x_o,t)$. Using 160 equally spaced values of $x_o$ on $[0,1]$ and Simpson's rule to integrate (26) numerically for $t^2 = .14$ produced a result which differed by only 0.02 per cent from the correct value $X = 3\pi/16$.

For the 3/2-power lift distribution that we have treated, the vortex sheet is an analytic curve for $|x_o| \leq 1$ in the initial stages of motion. A singularity, that is always present on the analytic continuation of the sheet, i.e. $|x_o| > 1$, moves inward as time progresses and arrives at $x_o = 1$ when $t^2 = t_*^2$.

The nature of the singularity and the corresponding value of $t_*^2$ can be estimated by use of a graphical procedure due to Domb & Sykes (1957). They note that if

$$f(\varepsilon) = \sum_{n=o}^{\infty} a_n \varepsilon^n = \kappa(\varepsilon_* - \varepsilon)^{\alpha} \ , \ \alpha \neq 0, 1, \ldots \tag{29a}$$

then

$$a/a_{n-1} = \varepsilon_*^{-1} [1 - (1 + \alpha)/n] \tag{29b}$$

which follows from the binomial expansion. Thus, for these special cases, if we plot the ratios $a_n/a_{n-1}$ versus $1/n$, the points will be on a straight line. In general the unknown function $f$ can be thought of as the sum of a number of singularities; if the one closest to the origin of $\varepsilon$ is of the above type, then the "Domb-Sykes plot" will ultimately tend towards a straight line as $1/n$ becomes small. Values of $\varepsilon_*$ and $\alpha$ appropriate to this singularity can be found

from the inclination and intercept of this straight line. When only a finite number of ratios are know, estimates of $\varepsilon_*$ and $\alpha$ can still be made if the plotted points tend towards a straight-line asymptote. It has not generally been recognized that (29) is still valid for complex values of $a_n$, in which case the asymptote will be a straight line in $(1/n, \mathcal{R}e\{a_n/a_{n-1}\}, \mathcal{I}m\{a_n/a_{n-1}\})$-space.

At the tip of the sheet, $x_o = 1$, the coefficients in the $t^2$-series for $x$ and $y$ in equations (5) have been used to construct the ratios $A_n(1)/A_{n-1}(1)$ and $B_n(1)/B_{n-1}(1)$. They are given in Table I. While each set of ratios appears to tend towards a limit, a careful examination reveals that these limits, if they exist, are somewhat different. Because of the intimate coupling between the two series implied by the governing equations (4a, b), this difference in the limits is unacceptible. That is, for a given value of $x_o$, the series for $x$ cannot converge for certain values of $t^2$ while the series for $y$, which is derived from it, diverges for these values. A more consistent interpretation is obtained by considering the complex series for the quantity

$$x(1,t) + i\, y(1,t)/t = \sum_{n=o} [A_n(1) + iB_n(1)]t^{2n} \equiv \sum_{n=o} C_n(1)t^{2n} \quad . \qquad (30)$$

The real and imaginary parts of the ratio $C_n(1)/C_{n-1}(1)$ are given in Table II and are also plotted in Figure 3. The abscissa has been taken as $1/(n + 5/4)$; the shift in $n$, related to the local behavior of a regular function which multiplies the singular one near $t_*^2$ is determined so as to minimize the curvature in the real-ratio

plot. The straight line shown in the figure has the equation

$$\mathcal{R}e\left\{C_n/C_{n-1}\right\} = \frac{1}{6.7286}\left[1 + \frac{5/2}{n + 5/4}\right] .$$

This line provides a virtually perfect fit to the ratios for $n \geq 7$. The points corresponding to the small imaginary part of the ratios do not lie on a straight line. They can be fitted to a smooth curve, however, which plausibly can be extrapolated to the origin. Near the critical value $t_*^2 = 0.14862 + i\ 0.0$, the left side of (30) varies locally like

$$R_1(t^2) + R_2(t^2)\left[1 - \frac{t^2}{t_*^2}\right]^{3/2-.067i} . \qquad (31)$$

The imaginary part of the exponent is estimated from the slope of the curve fitting $\mathcal{I}m\{C_n/C_{n-1}\}$ at the origin. Consequently, its value connot be considered as accurate as $\mathcal{R}e\{\alpha\} = 3/2$ . Because of the shift in the horizontal axis in Figure 3, the regular function $R_2$ probably behaves locally as $t^{-5/2}$. The regular functions $R_1$ and $R_2$ could be estimated by comparing the model equation (31) with the original series but this has not been attempted.

From the model function (31) the local behavior of the vortex sheet, specifically the trajectory of the sheet tip, may be deduced. Let

$$Z = Re^{i(\theta-\theta_o)} = A\left[x(1,t) - x(1,t^*) + i\ \frac{\{y(1,t) - y(1,t^*)\}}{t^*}\right]$$

$$= 1 - \left(\frac{t}{t^*}\right)^2 \quad \exp\left\{-.067i\ \ell n\ \left[1 - \left(\frac{t}{t^*}\right)^2\right]\right\} \qquad (32)$$

where $A$ and $\theta_o$ are real constants, representing the dilatation and rotation necessary to match the local behavior to the "outer" solution. Equation (32) represents a spiral of the form

$$(\theta - \theta_o) = -.0671 \ln R^{2/3}$$

or

$$R = e^{-22.4(\theta-\theta_o)} . \qquad (33)$$

Unlike Kaden's (1931) similarity solution for the tip region of the vortex sheet shed by an elliptically-loaded wing, $R = K/\theta^{2/3}$, which is a tightly-round spiral of infinite length, (33) represents a loosely-wound spiral whose length, as $\theta$ varies from $\theta_o$ to infinity, is finite. The numerical constant in (33) shows that in one revolution the spiral radius decreases by about 60 orders of magnitude!

Taking the time derivative of (31) reveals that the velocity components remain finite as $t \to t^*$ at the sheet tip. Since the sheet is continuous for all $t \leq t^*$, the spiral in (33) can also represent the spacial form of the sheet in the neighborhood of the tip at $t = t^*$. Because of the exponential character of the spiral and its very loose winding, it is not surprising that the roll-up cannot be observed in the sheet configurations in Figures 1 and 2.

As mentioned above, the radius of convergence of the series in time varies with $x_o$. The procedure used to predict $t_*^2$ for $x_o = 1$ was also employed for $x_o = 0.999$ and 1.001 to yield the first-order variation

$$t_*^2 (x_o) \tilde{=} .14862 - 2.88(x_o - 1)$$

near $x_o = 1$. For significantly smaller values of $x_o$, the ratio-plot procedure did not give accurate results, presumably due to the complexity of the pattern of singularities. It is clear, however, that the radius of convergence increases as $|x_o|$ is reduced. For values of $t^2$ greater than .14862, the series solution cannot predict the evolution of the vortex sheet because the vorticity distribution is no longer analytic on it. One may conjecture however that the vorticity between the critical value of $x_o$ and $x_o = 1$ becomes concentrated at the center of the spiral. The amount of vorticity at this point will increase with time; if, ultimately, all the vorticity becomes concentrated there, this point must lie at the centroid location, $X = 3\pi/16$, and will move downward with the constant speed predicted for a counter-rotating vortex pair.

As the sheet deforms from its initially flat configuration, vorticity is convected outward towards the tips. The vortex intensity is given by

$$\tilde{\kappa}(s,t) = \kappa(x_o)/(ds/dx_o) \tag{34}$$

which varies as the sheet is stretched. Since

$$\left(\frac{ds}{dx_o}\right)^2 = \left(\frac{\partial x}{\partial x_o}\right)^2 + \left(\frac{\partial y}{\partial x_o}\right)^2 ,$$

the stretching may be computed using Padé sums for the series $\sum_n A_n'(x_o)t^2$ and $t\sum_n B_n'(x_o)t^{2n}$. Figure 4 shows $dx/dx_o$ plotted versus $x_o$ for $t^2 = 0$, 0.05 and 0.148. Combining these results with $\kappa(x_o)$ gives $\tilde{\kappa}(s,t)$ according to (34). It is plotted versus

$x$ in Figure 5. Note that $\tilde{\kappa}$ is a double-valued function of $x$ near the tip for $t^2 = 0.148$ because the sheet has bent back towards the center.

We shall now consider formal power series solutions for vortex sheets whose vorticity distributions differ slightly from that produced by elliptic loading. For strictly elliptic loading, the airfoil integral (7) predicts constant downwash velocity on the open interval $x_o \in (-1, 1)$. To the extent that we restrict consideration here to analytic sheet configurations, the "formal" series solution is simply

$$\begin{aligned} x(x_o,t) &= x_o \quad , \\ y(x_o,t) &= -\frac{1}{2}\, t \quad . \end{aligned} \tag{35}$$

This "solution" is incomplete, however. As $x_o \to 1^+$, for example, infinite upwash results. Because the induced velocities are not continuous at the tips, the vortex sheet will not be analytic there. Because the discontinuity is infinite, moreover, the vertical induced velocity at $t = 0$ must include, at leading order, a singularity of the nature of a Dirac $\delta$-function there. This infinite velocity, directed at right angles to the tangent to the sheet, causes the tip to roll up intantaneously into the similarity form predicted by Kaden. The solution (35) is valid however at sufficient distance from the tips for sufficiently small time. It is, in essence, an "outer solution" which must be joined in some way to Kaden's description of the, initially small, vortex core.

Similar "outer" solutions can be produced by the present method for slightly perturbed elliptic distributions. Using the algorithm described in §2, we consider the two distributions

$$\kappa_1(x_o) = \frac{15x}{14\sqrt{1-x_o^2}}\left(1 - \frac{x^2}{10}\right) \tag{36a}$$

and

$$\kappa_2(x_o) = \frac{15x}{16\sqrt{1-x_o^2}}\left(1 + \frac{x^2}{10}\right) \quad . \tag{36b}$$

The series method generates the terms forced by these vorticity distributions using the integrals (7); the resulting solution is, of course, incomplete but fills the same role as does (35) for the pure elliptic case.

Figure 6 shows the shape of the sheet, computed by the Padé method, at a later time, for each distribution in (36). In both cases, the time series possess finite radii of convergence; again convergence fails first at the tips. The horizontal location of the centroid is not invariant for these incomplete solutions.

## REFERENCES


Birkhoff, G. & Fisher, J., 1959, Do vortex sheets roll up? *Rend. Circ. Mat. Palermo, Sec* 2, 8, 77-90.

Cabannes, H. (ed.), 1976, Padé approximants method and its application to mechanics. Berlin: Springer.

Chorin, A. J. & Bernard, P. S., 1973, Discretization of a vortex sheet with an example of roll-up. *J. Comp. Phys.* 13, 423-429.

Domb, C. & Sykes, M. F., 1957, On the susceptibility of a ferromagnetic above the curie point. *Proc. Royal Soc. London A*, 240, 214-228.

Fink, P. T. & Soh, W. K., 1974, Calculation of vortex sheets in unsteady flow and applications in ship hydrodynamics. *Proceedings of the 10th Symposium on Naval Hydrodyn.*, 463-489, U. S. Office of Naval Research

Fink, P. T. & Soh, W. K., 1978, A new approach to roll-up calculations of vortex sheets. *Proc. Royal Soc. London A*, 362, 195-209.

Kaden, H., 1931, Aufwicklung einer ustabilen unstetigkeits fläche. *Ingen. Arch.*, 2, 140-168.

Muskhelishvili, N. I., 1959, Singular integral equations. Wolters-Noordhoff Publishing, Groningen.

Prandtl, L. & Betz, A., 1927, Vier Abhandlungen zur hydro-und aerodynamik, Gottingen.

Rosenhead, L., 1931, The formation of vortices from a surface of discontinuity. *Proc. Royal Soc. London A*, 134, 170-192.

Spreiter, J. R. & Sacks, A. H., 1951, The rolling-up of the trailing vortex sheet and its effect on the downwash behind wings. *J. Aero. Sci.* 18, 21-32.

Takami, H., 1964, A numerical experiment with discrete-vortex approximation, with reference to the rolling-up of a vortex sheet. AFOSR 64-1536 (SUDAER 202) Department of Aeronautics and Astronautics, Stanford University.

Westwater, F. L., 1935, The rolling-up of the surface of discontinuity behind an aerofoil of finite span. Aeronautics Research Council Reports and Memoranda, No. 1692.

TABLE I: Ratios of Coefficients from Equations (5) for $x_o = 1$

| n | $A_n(1)/A_{n-1}(1)$ | $B_n(1)/B_{n-1}(1)$ |
|---|---|---|
| 1 | -1.125 | -1.125 |
| 2 | .1875 | .825 |
| 3 | 5.025 | 3.5601 |
| 4 | 2.6980 | 3.4615 |
| 5 | 3.6734 | 4.0983 |
| 6 | 3.9945 | 4.4265 |
| 7 | 4.3389 | 4.7077 |
| 8 | 4.5869 | 4.9226 |
| 9 | 4.7915 | 5.0976 |
| 10 | 4.9584 | 5.2414 |
| 11 | 5.0979 | 5.3620 |
| 12 | 5.2161 | 5.4646 |
| 13 | 5.3176 | 5.5528 |
| 14 | 5.4055 | 5.6295 |
| 15 | 5.4826 | 5.6968 |
| 16 | 5.5505 | 5.7563 |
| 17 | 5.6110 | 5.8093 |
| 18 | 5.6650 | 5.8569 |
| 19 | 5.7137 | 5.8997 |
| 20 | 5.7577 | 5.9386 |

TABLE II: Ratios of Complex Coefficients $C_n(1)/C_{n-1}(1)$ from Equation (30)

| n | $\mathcal{R}e\left\{C_n(1)/C_{n-1}(1)\right\}$ | $\mathcal{I}m\left\{C_n(1)/C_{n-1}(1)\right\}$ |
|---|---|---|
| 1 | -1.125 | 0.0 |
| 2 | .4170 | .3060 |
| 3 | 3.6833 | -.4066 |
| 4 | 3.3434 | .2761 |
| 5 | 4.0558 | .1275 |
| 6 | 4.3911 | .1185 |
| 7 | 4.6827 | .0927 |
| 8 | 4.9031 | .0786 |
| 9 | 5.0820 | .0673 |
| 10 | 5.2286 | .0588 |
| 11 | 5.3513 | .0522 |
| 12 | 5.4554 | .0468 |
| 13 | 5.5448 | .0425 |
| 14 | 5.6225 | .0388 |
| 15 | 5.6906 | .0358 |
| 16 | 5.7508 | .0331 |
| 17 | 5.8044 | .0308 |
| 18 | 5.8524 | .0289 |
| 19 | 5.8957 | .0271 |
| 20 | 5.9349 | .0256 |

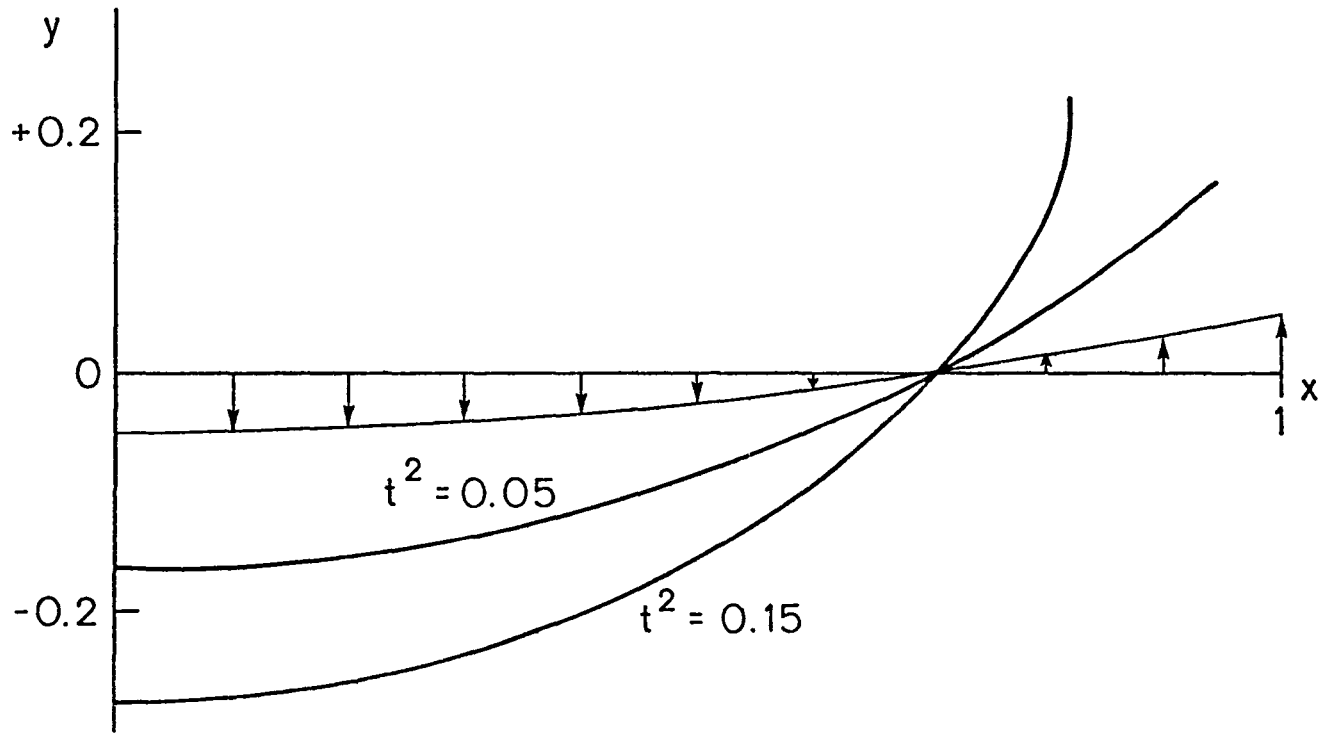


Figure 1. The vortex sheet configuration for 2 values of $t^2$; $\kappa(x_o) = 3x_o\sqrt{1 - x_o^2}$ .

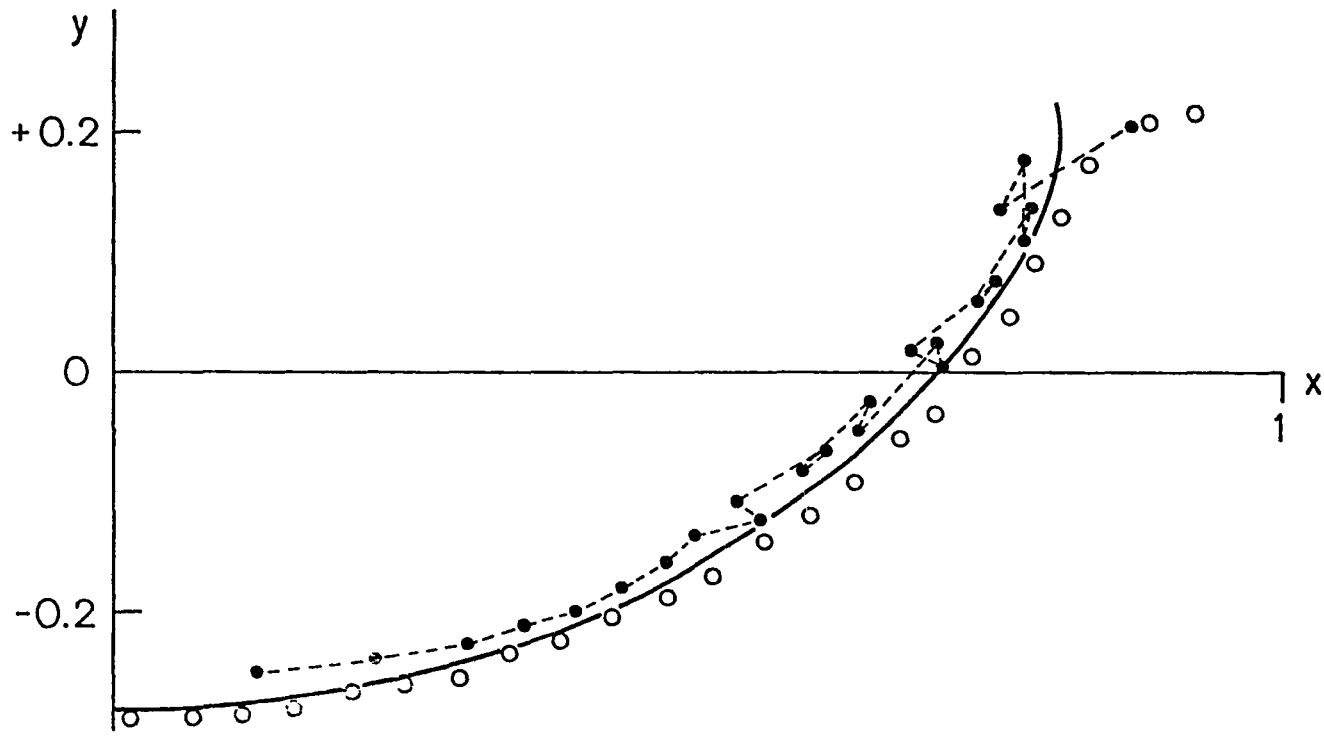


Figure 2. Comparison of present results with Takami, --•---•-, and Fink & Soh, o o o; $t^2 = .16$, $K(x_o) = 3x_o\sqrt{1-x_o^2}$ .

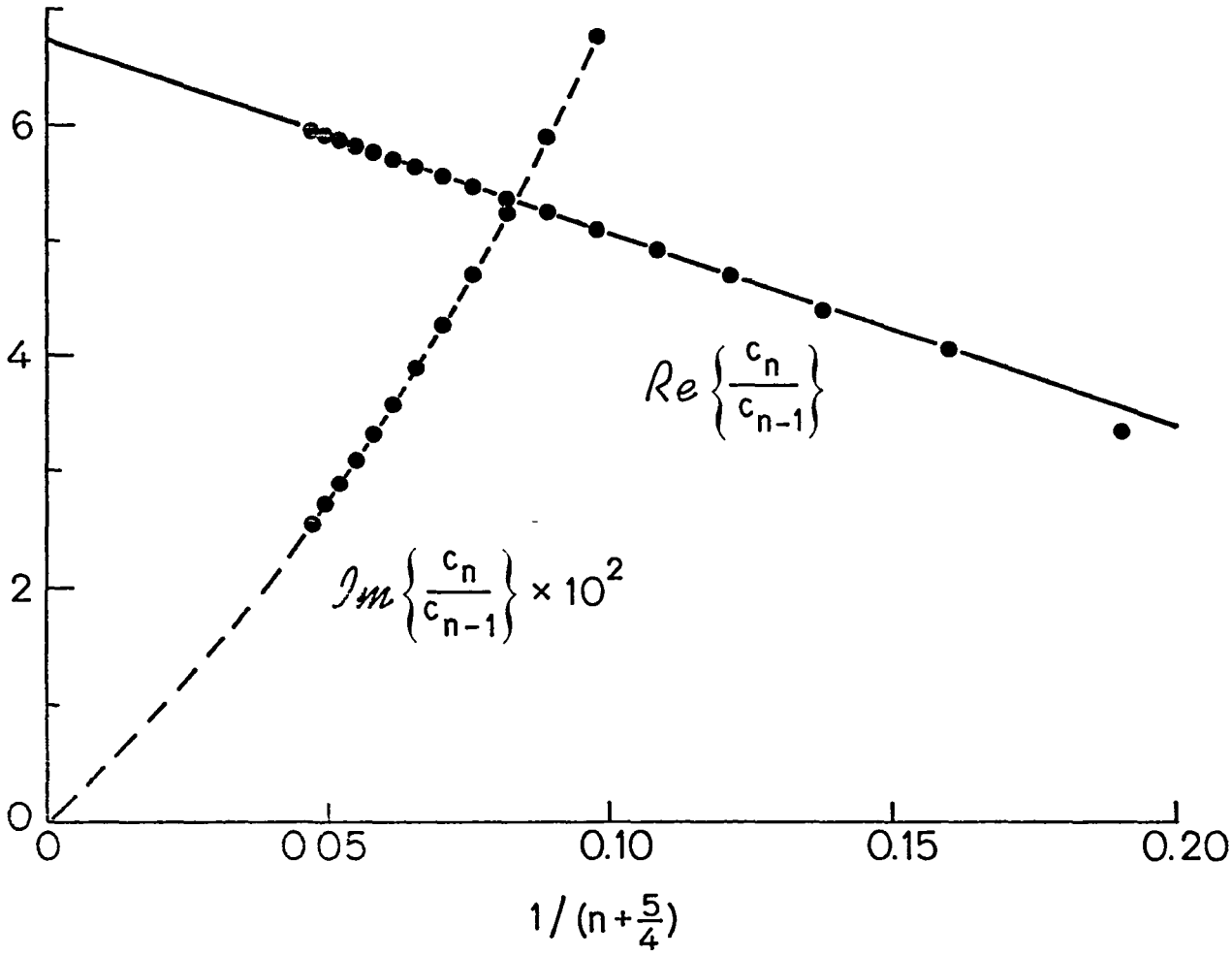


Figure 3. Domb-Sykes plots for the series $\sum_{n=0}^{\infty} C_n(1)t^{2n}$ in equation (30).

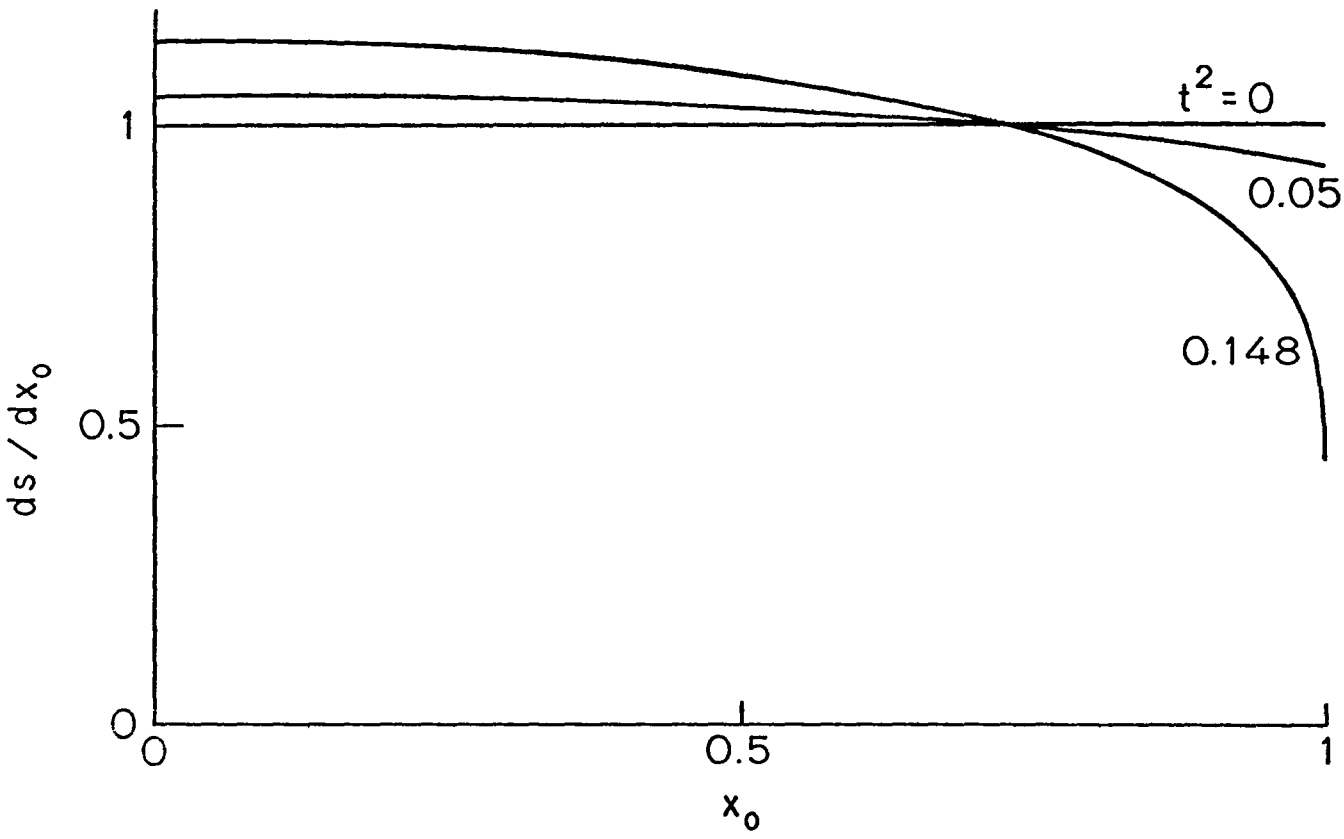


Figure 4. Vortex-stretching parameter for 3 values of time; $K(x_o) = 3x_o\sqrt{1 - x_o^2}$ .

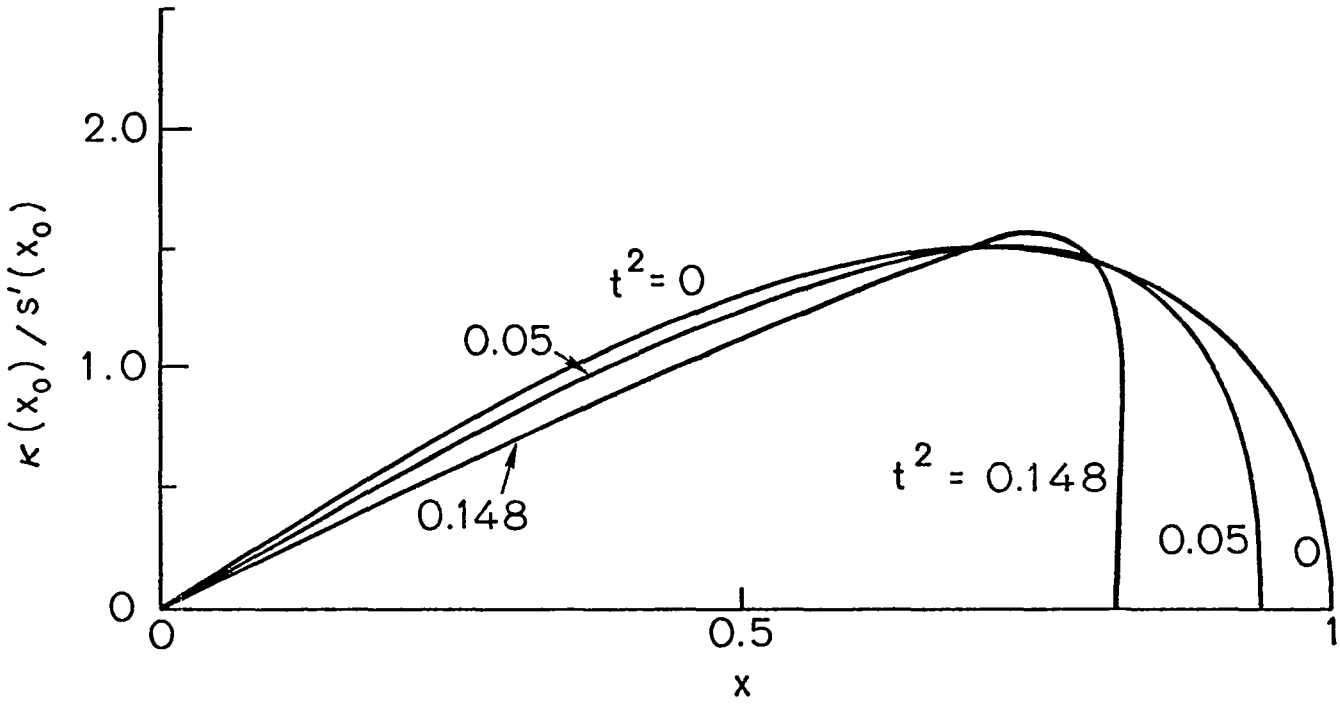


Figure 5. Variation of vortex sheet strength for 3 values of time; $\kappa(x_o) = 3x_o\sqrt{1 - x_o^2}$ .

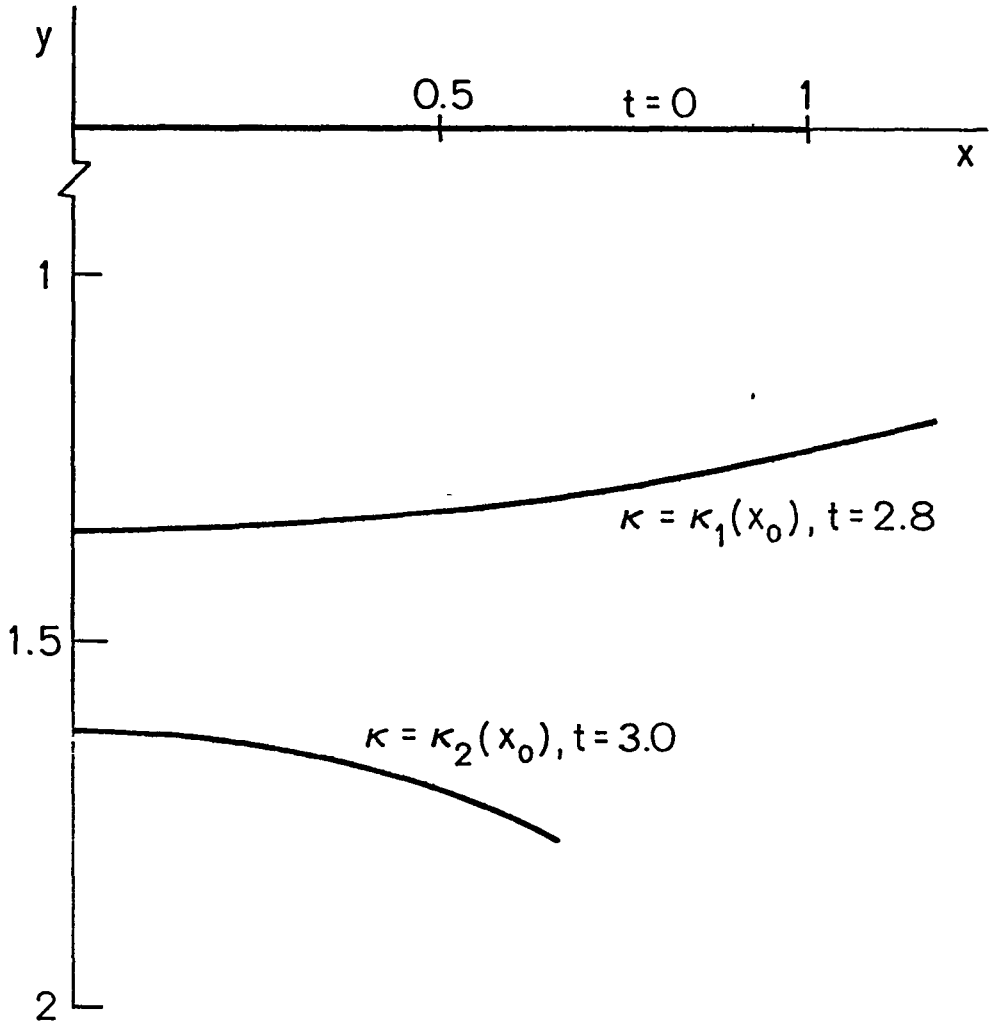


Figure 6. Sheet configurations from "incomplete" solution for perturbed elliptic distributions.

End of Document